Optical sorting and detection of submicrometer objects in a motional standing wave

Tomáš Čižmár, Martin Šiler, Mojmír Šerý, and Pavel Zemánek
Institute of Scientific Instruments, Academy of Sciences of the Czech Republic, Královopolská 147, 612 64 Brno, Czech Republic

Veneranda Garcés-Chávez and Kishan Dholakia
School of Physics and Astronomy, University of St. Andrews, North Haugh, Fife KY16 9SS, Scotland
(Received 6 September 2005; revised manuscript received 21 April 2006; published 10 July 2006)

An extended interference pattern close to the surface may result in either a transmissive or an evanescent surface field for large-area manipulation of trapped particles. The affinity of differing particle sizes to a moving standing-wave light pattern allows us to hold and deliver them in a bidirectional manner and demonstrate experimentally particle sorting in the submicrometer region. This is performed without the need of fluid flow (static sorting). Theoretical predictions support the experimental observations that certain sizes of colloidal particles thermally hop more easily between neighboring traps. A generic method is also presented for particle position detection in an extended periodic light pattern and applied to characterization of optical traps and particle behavior.

DOI: 10.1103/PhysRevB.74.035105 PACS number(s): 42.50.Vk, 42.25.−p, 82.70.Dd

I. INTRODUCTION

Optical trapping and guiding of micrometer- and submicrometer-size objects have been key topics for studies in the realm of mesoscale science in the last three decades.[1] A recent drive in the field is the ability to interact with large-scale ensembles of particles in two and three dimensions: interferometric patterns may help to achieve this. Light fields at or near total internal reflection may assist in allowing one to organize upwards of 1000 particles adjacent to a surface.[2,3] Recent work has shown the experimental demonstration of optical separation using extended optical lattice or holographic methods in the presence of a laminar flow[4,5] and it has been followed by theoretical analyses.[6] In these studies the particles are not trapped *per se* but rather their differing affinity to a periodic light pattern (landscape) is exploited. This sensitivity is very high and potentially offers a new noninvasive method for optical separation. A key advance would be to show how we may separate submicrometer objects in the absence of a flow and potentially over a large area, facilitating greater throughput. Near-field optical guiding or trapping[7–9] has shown the ability to potentially organize particles over areas of mm^2 and to offer prospects for sorting over a large region.[2,3,10] Tuning the incident angle from below to above the critical angle results in a transition between propagating and evanescent light fields. This geometry for such optical organization is eminently suitable for sorting, even if a small part of the incident focused beam is below the critical angle and thus forms a propagating field.

In this paper we present an interferometric system that provides confinement and longitudinal bidirectional controllable separation of microparticles (see Fig. 1). The experimental geometry permits evanescent wave confinement as well as confinement just above the surface (by judicious choice of incident angle via position of the obstructing edges E_1, E_2): this choice of geometry allows extension of the data presented here to a large area and concomitant higher throughput. The key result we show is the optical separation of submicrometer particles in the absence of any imposed flow by exploiting the varying affinity of objects to this spatially modulated light pattern (optical potential energy landscape). We are able to separate objects based upon their size. Furthermore, we demonstrate an original method for particle detection within this periodic near-field light pattern. This is applied here for quantitative study of submicrometer particle behavior but it can serve generically in any area where scattering of an imposed periodic light pattern by Brownian particles on a surface can be detected (interaction of colloids, colloidal dynamics, colloidal models of thermodynamic systems, optical manipulation and sorting).

II. EXPERIMENTAL SETUP AND RESULTS

The interference of two counterpropagating (CP) surface fields (combination of evanescent and propagating waves) at or near the critical angle creates standing waves (SWs) above or at the surface (x-z plane; see Fig. 1). As our data apply for interfering both evanescent and propagating waves we generally term this effect a surface standing-wave (SSW) field. In contrast to previous methods[11,12] we used a setup with two independent CP Gaussian beams where the phase between them can be precisely controlled by the position or movement of the mirror MM (see Fig. 1). These beams were focused on the top surface of the prism to form two overlapping spots each of area $40\times 10\ \mu m^2$. In comparison to the single-beam case of the same intensity, the interferometric optical potential well is deeper and steeper and consequently gives a stronger longitudinal force component.[13] The final result is that smaller particles can be confined and transported rapidly in both longitudinal directions if the SSW is moved by changing the phase between the two beams. It results in a surface optical conveyor belt (OCB). This is related to recent work in sliding SWs using radiative fields for atom delivery,[14–16] submicrometer particle delivery using Bessel beams,[17] or the use of vibrating fringe patterns.[18]

In this manner we were able to move a range of particles from 350 to 800 nm in size over a range of 36 μm on the surface [Fig. 2(a)]. However, particles of sizes 410 and 750 nm in contrast did not follow the moving SSW and were unaffected by its presence [see Figs. 2(b) and 2(c)].

Based on our previous work[13,19] we examine this behavior with a theoretical study of optical forces based on a Lorentz-

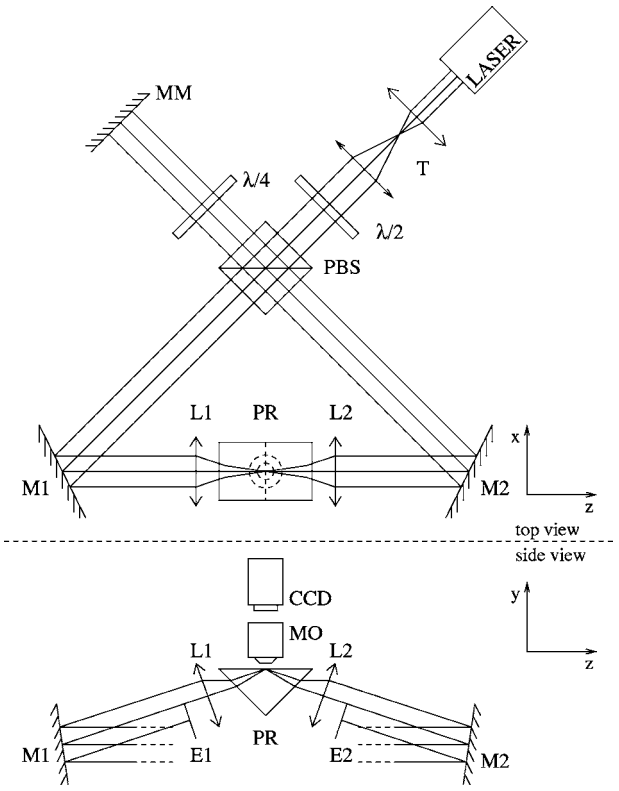

FIG. 1. Experimental setup. A linearly polarized beam (Verdi, 5 W, λ_{vac}=532 nm) is three times enlarged passing through telescope *T*; the following half-wave plate $\lambda/2$ rotates the polarization so that the beam is separated into two parts. One is reflected on the polarizing beam splitter (PBS), changed to circularly polarized on a $\lambda/4$ plate, reflected on the movable mirror MM, and changed to a linearly polarized beam after passing again through the $\lambda/4$ plate. Its polarization is now perpendicular to the original one reflected to this arm and so the beam passes through the PBS to the mirror M2 and is focused by lens L2 on the surface of the prism PR. The second beam passed through the PBS, the mirror M1, and the lens L1 and overlaps on the top surface of the prism PR with the first beam. On the lower plot the side view shows the obstructing edges E1 and E2. They block the wave vectors in the plane wave spectrum of the incident field that forms the radiative wave above the surface. At the same time the evanescent field was generated mainly by the high-intensity core of the Gaussian beam. Overlapping of both beams gave a spot 40 μm long and 10 μm wide with standing-wave fringes separated by 200 nm. Movable mirror MM was controlled by a piezoelectric controller (PiFoc, Physik Instrumente) which provided precise and fast movement over 150 μm.

Mie scattering model[20] modified for CP evanescent waves created from two incident plane waves. This model does not include either the Gaussian spatial beam profile or the surface interactions for the scattered light. Note that surface interactions mainly affect the force component perpendicular to the surface and only up to a distance about 50 times smaller than the trapping wavelength.[21] Therefore they are not the dominant consideration for the work presented here. Figure 3 shows theoretical depths of the optical traps and illustrates the selectivity of the SSW to various sizes of microparticle. The lighter shaded regions indicate deep traps where the objects can be confined with smaller requirements on beam intensities. The darker regions correspond to shallow traps and in accordance with the lower beam intensity the object resides only briefly in these regions and hops due to thermal activation to a neighboring trap site. The sphere sizes affected and unaffected by this phenomenon do not strongly depend on the considered incident angle of the plane waves. Experimentally our observations concur with the above theory for monodisperse (in size) or diluted samples on the top of the prism and we can readily observe the differing affinity of the particles to a SW pattern similar to Figs. 2(b) and 2(c). However, dense colloidal samples may suffer from interparticle interactions. An example of this can be seen in Fig. 2(c) where the insensitive larger particle starts to move even before physical contact with the smaller particle. This is attributed to an optical binding type of interaction[22–24] where scattered light from the particle selected by the OCB affects the optical forces experienced by the unaffected particle.

To exploit the above selectivity for separation of microparticles according to their size we exposed diluted samples to a tilted washboard potential,[25] created by introducing a slight intensity asymmetry between the two CP beams. This asymmetry created a differential optical gradient along the SW and motion of this pattern resulted in the particle sorting demonstrated in Fig. 4. In connection with Fig. 3 it also reveals how we may even extend this technique to sort objects of different sizes (see Figs. 5 and 6). This demonstrates that the method is able to separate objects of sizes differing by just 60 nm.

III. PARTICLE TRACKING AND OPTICAL TRAP ANALYSIS

To explore in detail the properties of the SSW we present an original method of particle detection within this optical landscape. The basis for this method lies in changes of the observed light pattern created by the scattered light in the plane of a CCD camera when the mutual configuration of the particle and SSW is altered (see Fig. 7). Since the SSW has a sinusoidal intensity dependence along the propagation axis, the intensity at each pixel of the CCD camera has to follow this sinusoidal dependence when the particle moves over several SSW periods. As described below we found parameters for these sinusoidal dependences for each pixel of the CCD camera and these functions enabled reconstruction of the interference pattern for each longitudinal position of a particle in the SSW. Consequently, these calculated patterns can be compared with a measured pattern while the particle moves in the fixed trap. To determine the particle coordinates from the tracking record, we need to determine for each frame the reconstructed pattern of the correct shape and attribute it to the right position. This is achieved using the translation property of fast Fourier transform. This procedure gives us two pieces of information regarding the longitudinal particle position—one with respect to the CCD (from the image shift) and the other with respect to the the SSW (from the pattern shape). The latter of these can be obtained with nanometer resolution regardless of the stability of the SSW with respect to the CCD. Unfortunately this is not true for

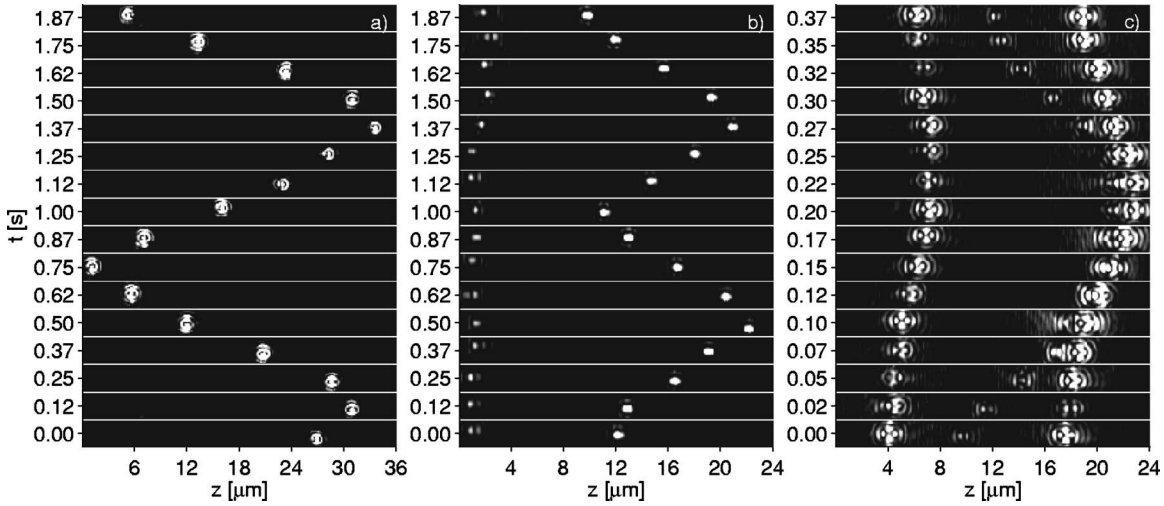

FIG. 2. Particle delivery and particle affinity to the optical conveyor belt (OCB). (a) A polystyrene sphere of diameter 520 nm is delivered over a distance of 36 μm. (b) Mixture of spheres of sizes 410 nm (left) and 520 nm (right). While the larger move with the OCB, the smaller keep their original position unaffected by the OCB. (c) Mixture of polystyrene particles of diameters 350 and 750 nm where the smaller one follows the OCB motion. The larger sphere remains unaffected until it is in close proximity to the smaller sphere ("binding" interaction).

the lateral direction, which can only be found from the image shift. Experimentally the sinusoidal functions for each CCD pixel were found first from a fast sweep of the SSW over the particle, such that the particle did not change its position. Second, the particle motion in a stationary trap was recorded and analyzed. Both steps were performed within 3.27 s of one recording by a fast CCD camera (IDT X-Stream XS3, 4 GB) where 20 000 frames were taken. We used the same frame rate equal to 6120 fps and an integration time in the range from 2 to 8 μs with the time adjusted according to the size of the particle.

In the subsequent experiments we tuned the beam incident angle so the transmissive field was negligible and therefore we could assume an exponential decay of the SSW above the surface. The estimation of the relative particle position above the surface was made in three steps for each measured frame. First we calculated the image to best fit the pattern of the measured one. Therefore we found the position of the sphere in the SW and the z, x positions. Second, the ratio of the total image intensity (sum over intensities of all pixels) of measured I_m and calculated I_c images was calculated. The calculated image is related to one fixed sphere position above the surface. Since we assume the exponential decay of the field above the surface, a linear relation was expected: $\ln(I_m/I_c) \simeq A+By$. Third, the velocity distributions along the z and x axes were calculated as the histograms of the differences between the measured points. Along the y axis the differences between neighboring values of $\ln(I_m/I_c)$ were taken to the histograms. These distributions have to be the same for all axes because the sampling rate is much smaller than the rate at which the thermal equilibrium of velocity distributions is established ($\simeq 6\pi\eta a/m$, where η is the water

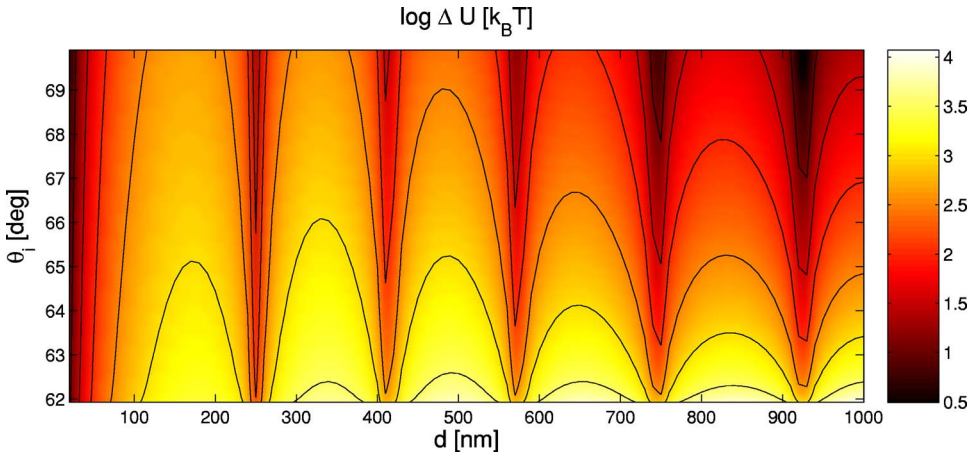

FIG. 3. (Color online) Theoretical results showing how the longitudinal trap depth in the SW formed by the CP near field depends on the diameter of the polystyrene sphere and on the incident angle of the plane waves (the same for both CP waves) upon the prism surface. The trap depth is in logarithmic scale (see the bar for units). The contour lines show the trap depths of $33kT$, $100kT$, $333kT$, $1000kT$, and $3333kT$. Polarizations of both beams are normal to the plane of incidence, i.e., parallel with the prism surface; the amplitude of a single plane wave electric field is the same as it is in the center of a 1 W Gaussian beam focused to a beam waist 1 μm ($E=1.9\times10^7$ V/m).

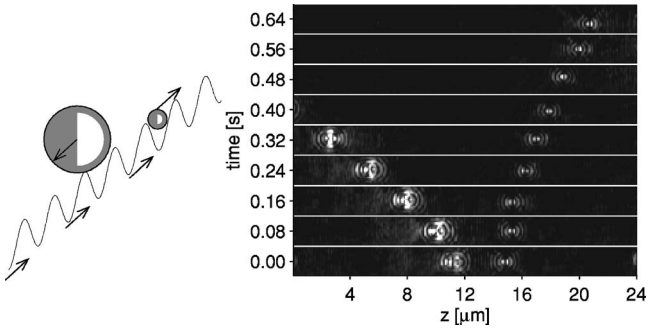

FIG. 4. An example of our method of optical sorting of colloids. The imbalance between the intensities generates imbalance between the radiation pressures coming from the two CP beams and tilts the landscape. Consequently, the particles that are not affected by the SSW (dark regions in Fig. 3) are guided in the direction of the tilted washboard potential (to the left here). In contrast, the spheres affected by the SSW (the lighter regions in Fig. 3) follow the motion of the SW and they are delivered against the tilted potential landscape. The sample presented here consisted of a mixture of polystyrene particles of diameter 750 nm (left, insensitive to SSW) and 350 nm (right, sensitive to SSW) dispersed in water.

viscosity, and a and m are the sphere radius and mass, respectively, ignoring as a first step the Faxen correction due to surface proximity[26]). Using this assumption we obtained the calibration factor B of the y axis as the fit to the velocity distribution along the z axis. An example of the results obtained is shown in Fig. 8 in the form of histograms of 10^4 particle positions taken within 1.63 s.

To determine the longitudinal trap depths ΔU for each of the measured particle sizes we used the particle positions z_ψ

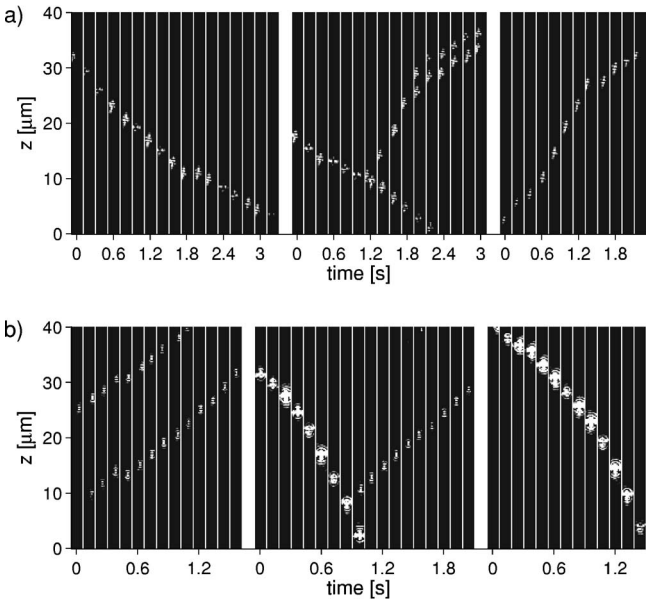

FIG. 5. Examples of sorting of colloids of different sizes. Polystyrene beads of diameters 350 and 410 nm in (a); 350 and 750 nm in (b). The beads of diameter 350 nm are delivered by the conveyor belt in the positive direction of the z axis; the others are insensitive to the periodic modulation of the potential (see Fig. 3) and therefore they fall down due to the tilt of the washboard potential.

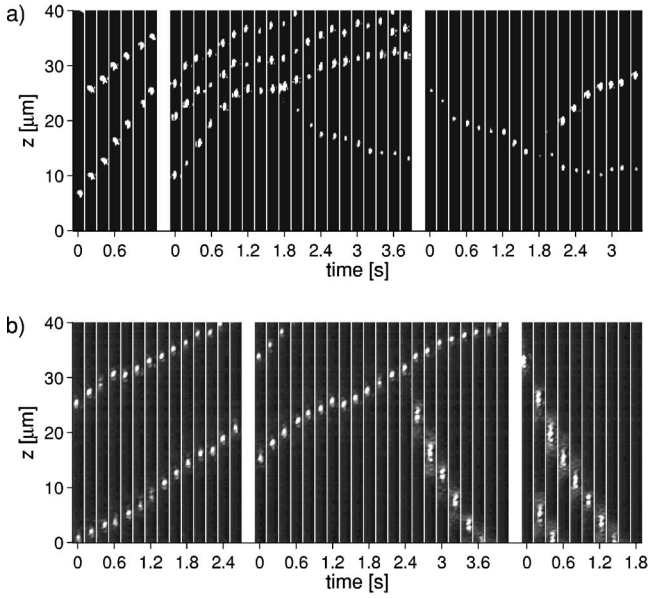

FIG. 6. Examples of sorting of colloids of different sizes. Polystyrene beads of diameters 410 and 520 nm in (a); 520 and 750 nm in (b). The beads of diameter 520 nm are delivered by the conveyor belt in the positive direction of the z axis; the others fall down due to the potential tilt because they are insensitive to the periodic modulation of the washboard potential (see Fig. 3).

(with respect to the SW position) obtained from the shape of the interference pattern. Since these positions are obtained in units of the intensity spatial period, we constrained them into the interval of one trap extent $z_\psi=(-1/2,1/2)$ and we made a histogram on this interval. Then we fitted to the histogram the Boltzmann distribution[27] in the form $A\exp[-\Delta U^*\sin^2(\pi z_\psi+b)/(k_BT)]$ with unknown parameters A, ΔU, b, and fixed values of the temperature $T=300$ K and Boltzmann constant k_B. While we could not measure the optical intensity precisely, we kept the same laser power for each measurement which allowed us to keep the same intensity for all the particle sizes. This enabled us to compare the experimental results with the theoretical model in the following way. We calculated the trap depths for the particle sizes used in experiments for different incident angles of the plane waves. All plane waves had the same intensity and we looked for a single multiple of this intensity (the same for all sizes) that gave the best coincidence with the experimental results. Therefore only these two parameters—incident angle and field intensity—were the subjects of fitting and were assumed to be the same for all studied particle sizes. The rest

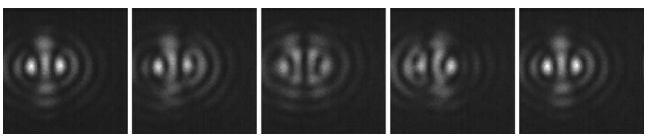

FIG. 7. An example of five images of a 520 nm particle taken during fast sweep of the SSW over the particle. The particle was assumed to be stationary and uninfluenced by the SSW motion. The first and the last images correspond to the particle equilibrium position.

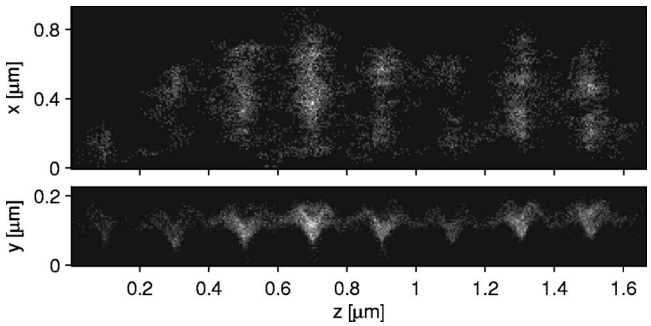

FIG. 8. Histograms of particle (diameter 600 nm) positions showing eight distinct optical traps. Each trap is much narrower in longitudinal direction (z) comparing to the lateral one (x) (see the top image). The bottom image describes how the object behaved in the z and y axes. The further one is from the surface (y axis), the wider the spread in the z distribution. The trapping field exponentially decays in this direction and so the object was not so tightly localized.

of the parameters—particle size, refractive indices of the prism ($n_{pr}=1.5098$) and polystyrene object ($n_o=1.59$), wavelength in vacuum $\lambda_{vac}=532$ nm and temperature $T=300$ K—were fixed. Figure 9 shows the results of this procedure for two sets of measurements with different incident angles and laser intensities. The following values of plane wave incident angles θ_i and field intensities E were found: for the first arrangement (+ markers) $\theta_{i1}=62.008°$, $E_1=5.84\times10^{10}$ V/m and for the second arrangement (○ markers) $\theta_{i2}=61.92°$, $E_2=7.28\times10^{10}$ V/m. Full and dashed curves show the theoretical results for all nonmeasured particle sizes if the parameters mentioned above were used. Once the trap depth ΔU is known, the longitudinal stiffness κ of optical traps can be obtained from $\kappa=8\pi^2 n_{pr}^2 \Delta U \sin^2\theta_i/\lambda_{vac}^2$. The difference in incident angles is small such that $(\sin\theta_{i1}/\sin\theta_{i2})^2\simeq1.003$. Thus we can use the same scale of the trap stiffnesses for both measurements in Fig. 9. Noting that the experiments involved Gaussian beams and the theoretical model considered two identical plane waves with only two free parameters for the fit, we believe that the agreement obtained is fairly good. Moreover, the determined values of θ_i are slightly bigger than the critical angle for total internal reflection for the studied configuration ($\theta_{icrit}=61.9132°$). This indicates that the experimentally generated field was evanescent in this case.

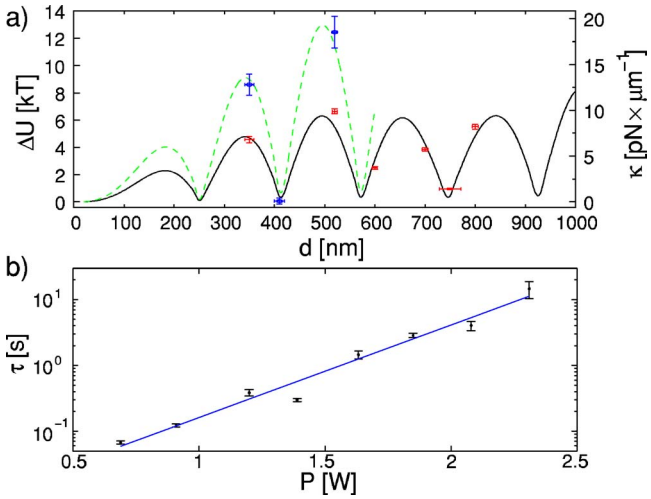

FIG. 9. (Color online) (a) Calculated (full and dashed lines) and measured (+ and ○) depths of the optical traps in the longitudinal direction. The dashed line is for a setup with slightly smaller incident angle. The vertical error bars coincide with the 95% confidential level and the horizontal ones express the standard deviation of the size of the experimentally used particles. (b) Dependence of the mean first passage time τ for a polystyrene bead of diameter 520 nm from one trap to neighboring trap in the SSW on the power of the trapping laser. These values were taken from 100 to 500 jumps and each value of τ in the figure came from a fit of an exponential distribution of the first passage times of an object from the trap: $\exp(-t/\tau)/\tau$ (Ref. 28). The error bars show the confidence level of 95% for the fitted time constants τ.

The stochastic processes of Brownian motion dictate the particle dynamics. We measured how the mean first passage time (MFPT) from one trap to the neighboring trap depends upon the laser power [see Fig. 9(b)]. Assuming an exponential distribution for passage time,[28] the MFPT also corresponds to the period during which only $100\exp(-1)\%\simeq36.8\%$ of the particles stayed in the same trap.

IV. CONCLUSION

This system may have potential for the organizing of biological and colloidal submicrometer objects localized on the surface. Characterization of the trap properties in the periodic surface light patterns showed that the trap depths and the residence time for the particle in the trap varies significantly with the particle size. In dense samples, with particle mixtures both sensitive and insensitive to the SSW, an optical "binding" interaction between adjacent particles was seen. This in itself may deliver even insensitive particles with the particles confined in the sliding SSW. The affinity of the particle size for the moving SSW was used to show how diluted solutions of submicrometer colloids can be optically sorted without fluid flow by exposing the particles to a suitable optical washboard potential. If the objects in the sample were further apart and we had more laser power at our disposal, we might readily expand the laser spot to cover an area of mm^2 or larger to potentially sort a greater number of objects. Finally, we note that analogous calculations to those presented show that sorting may also occur due to variations in refractive index between particles of exactly the same physical dimensions.

ACKNOWLEDGMENTS

This work was partially supported by the EC 6FP NEST ADVENTURE Activity (ATOM3D, Project No. 508952), ISI IRP (Grant No. AV0Z20650511), GA ASCR (Grant No. IAA1065203), MEYS CR (Grant No. LC06007). K.D. acknowledges support by the European Science Foundation EUROCORES program SONS (project NOMSAN), by funds from the U.K. Engineering and Physical Sciences Research Council, and by the EC Sixth Framework Program.

[1] M. J. Lang and S. M. Block, Am. J. Phys. **71**, 201 (2003).
[2] M. Gu, J.-B. Haumonte, Y. Micheau, J. W. M. Chon, and X. Gan, Appl. Phys. Lett. **84**, 4236 (2004).
[3] V. Garcés-Chávez, K. Dholakia, and G. C. Spalding, Appl. Phys. Lett. **86**, 031106 (2005).
[4] M. P. MacDonald, G. C. Spalding, and K. Dholakia, Nature (London) **426**, 421 (2003).
[5] K. Ladavac, K. Kasza, and D. G. Grier, Phys. Rev. E **70**, 010901(R) (2004).
[6] A. M. Lacasta, J. M. Sancho, A. H. Romero, and K. Lindenberg, Phys. Rev. Lett. **94**, 160601 (2005).
[7] S. Kawata and T. Sugiura, Opt. Lett. **17**, 772 (1992).
[8] S. Kawata and T. Tani, Opt. Lett. **21**, 1768 (1996).
[9] T. Tanaka and S. Yamamoto, Appl. Phys. Lett. **77**, 3131 (2000).
[10] R. Quidant, D. Petrov, and G. Badenes, Opt. Lett. **30**, 1009 (2005).
[11] M. Gu and P. C. Ke, Appl. Phys. Lett. **75**, 175 (1999).
[12] C. D. Mellor and C. D. Bain, ChemPhysChem **7**, 329 (2006).
[13] P. Zemánek, A. Jonáš, P. Jákl, M. Šerý, J. Ježek, and M. Liška, Opt. Commun. **220**, 401 (2003).
[14] P. Zemánek and C. J. Foot, in *Wave and Quantum Aspects of Contemporary Optics*, Proceedings of SPIE, Vol. 3320, edited by J. Nowak and M. Zajac (SPIE, Bellingham, WA, 1998), pp. 97–103.
[15] S. Kuhr, W. Alt, D. Schrader, M. Müller, V. Gomer, and D. Meschede, Science **293**, 278 (2001).
[16] I. Dotsenko, W. Alt, M. Khudaverdyan, S. Kuhr, D. Meschede, Y. Miroshnychenko, D. Schrader, and A. Rauschenbeutel, Phys. Rev. Lett. **95**, 033002 (2005).
[17] T. Čižmár, V. Garcés-Chávez, K. Dholakia, and P. Zemánek, Appl. Phys. Lett. **86**, 174101 (2005).
[18] I. Ricárdez-Vargas, P. Rodríguez-Montero, R. Ramos-García, and K. Volke-Sepúlveda, Appl. Phys. Lett. **88**, 121116 (2006).
[19] P. Zemánek, A. Jonáš, and M. Liška, J. Opt. Soc. Am. A **19**, 1025 (2002).
[20] E. Almaas and I. Brevik, J. Opt. Soc. Am. B **12**, 2429 (1995).
[21] M. Lester and M. Nieto-Vesperinas, Opt. Lett. **24**, 936 (1999).
[22] M. M. Burns, J. M. Fournier, and J. A. Golovchenko, Phys. Rev. Lett. **63**, 1233 (1989).
[23] S. A. Tatarkova, A. E. Carruthers, and K. Dholakia, Phys. Rev. Lett. **89**, 283901 (2002).
[24] N. K. Metzger, K. Dholakia, and E. M. Wright, Phys. Rev. Lett. **96**, 068102 (2006).
[25] S. A. Tatarkova, W. Sibbett, and K. Dholakia, Phys. Rev. Lett. **91**, 038101 (2003).
[26] J. Happel and H. Brenner, *Low Reynolds Number Hydrodynamics* (Prentice-Hall, Englewood Cliffs, NJ, 1965).
[27] E.-L. Florin, A. Pralle, E. H. K. Stelzer, and J. K. H. Horber, Appl. Phys. A: Mater. Sci. Process. **66**, 75 (1998).
[28] A. Simon and A. Libchaber, Phys. Rev. Lett. **68**, 3375 (1992).